Relativistic MHD simulations of Alfvén QPOs in magnetars

José A. Font

Departamento de Astronomía y Astrofísica

Universidad de Valencia (Spain)

Collaborators: Pablo Cerdá-Durán (MPA)

Nikolaos Stergioulas (AUTH)

Outline of the talk

Introduction: giant flares in SGRs

Framework

- Alfvén QPO model
- Semi-analytic approach

Numerical simulations

Conclusions

Cerdá-Durán, Stergioulas & Font, MNRAS accepted (2009)
(arXiv:0902.1472)

Giant flares in SGRs

Soft gamma repeaters: peaks of gamma-ray flare activity (10^{44}-10^{46} erg/s in ~0.2 s) followed by a decaying X-ray tail (~100 s)

SGRs are a class of magnetars (Duncan & Thomson 1992): neutron stars with very strong magnetic fields ($B>10^{14}$G)

Three giant flares have been detected so far:

- SGR 0526-66 on March 5, 1979
- SGR 1900+14 on August 27, 1998
- SGR 1806-20 on December 27, 2004

How magnetar bursts happen?

Magnetic-field-driven quakes in the crust of neutron stars

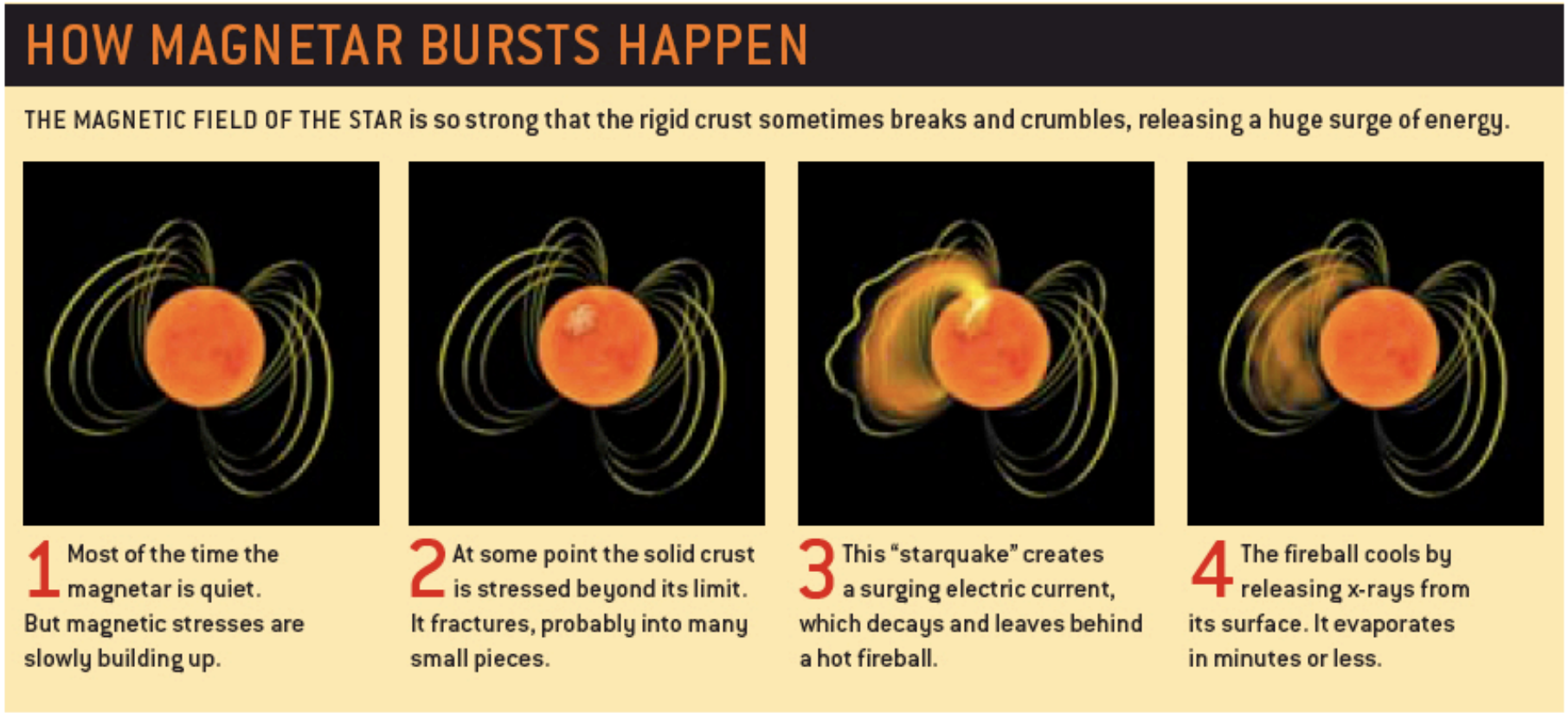

Kouveliotou, Duncan & Thompson, Scientific American (2003)

QPOs in the decaying X-ray tail

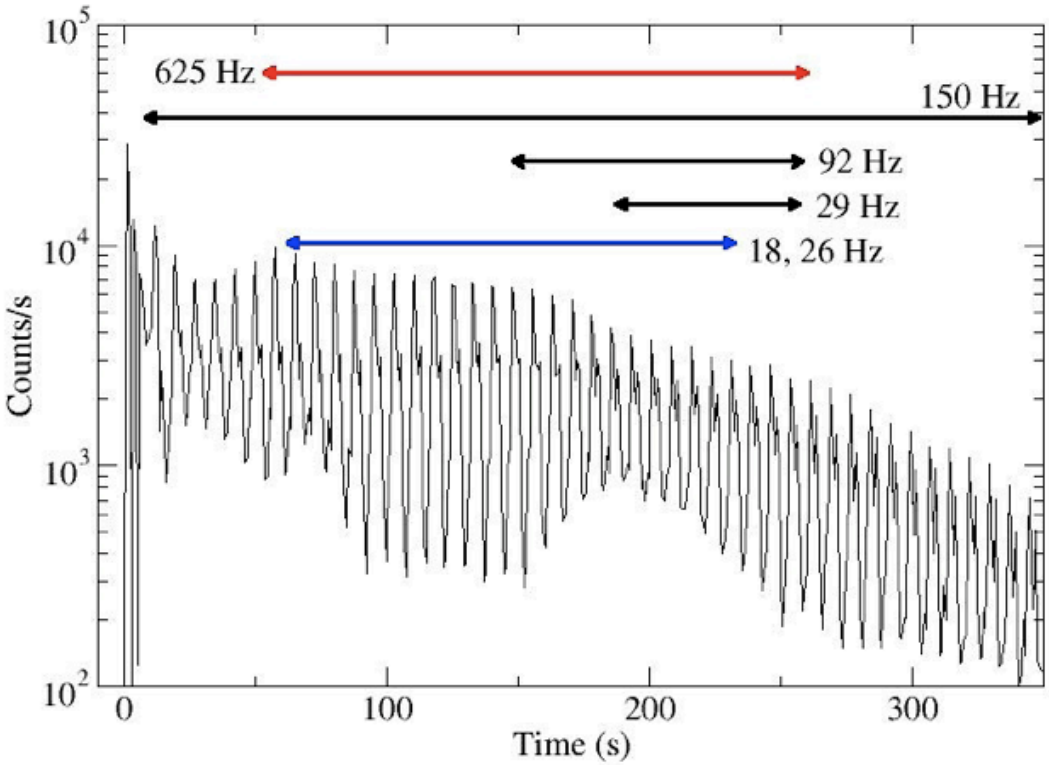

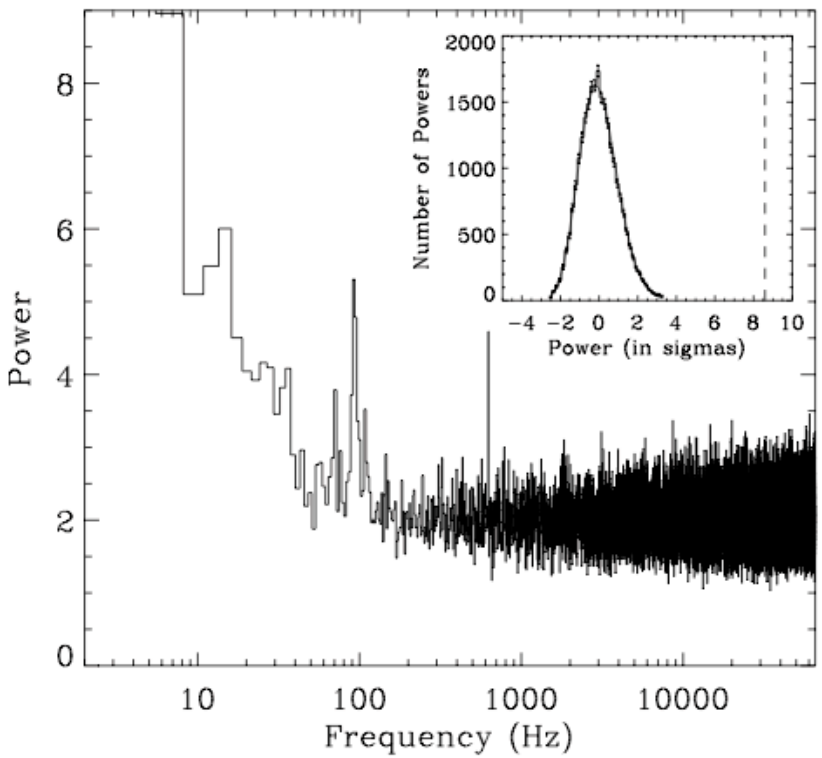

High frequency variations (QPOs) discovered in the tail of the 2004 flare from SGR 1806-20 using data from RXTE and RHESSI (Israel et al. 05, Watts & Strohmayer 06, Strohmayer & Watts 06).

Similar QPOs discovered in the tail of the 1998 flare from SGR 1900+14 using RXTE data (Strohmayer & Watts 05).

Model 1: torsional modes of solid crust

The QPO frequencies are in broad good agreement with models of torsional shear modes of neutron star crusts.

- Torsional shear oscillations of the crust, fundamental frequency ~30 Hz (Schumaker & Thorne 1983)
- Free slip models (crust moves independently of the core) (Piro 2005; Samuelsson & Andersson 2007)
- **Fail to explain all frequencies.**

SGR 1806-20	SGR 1900+14	Torsional shear mode identification
18*	?	
26*		
30*	28	$n=0,\ l=2$
	53	$n=0,\ l=4$
92*	84	$n=0,\ l=6$
150		$n=0,\ l=10$
	155	$n=0,\ l=11$
625*		$n=1$
1840		$n=3$

* detected in RXTE and RHESSI datasets.

Watts & Strohmayer 2006

Model 2: Alfvén QPO model

Both, global (crust-core coupling) elasto-magnetic oscillations and pure Alfvén oscillations.

Previous models:

- **Simplified geometry** (Glampedakis et al 2006; Sotani et al 2007)
  - Global Alfvén modes
  - Too simplified geometry
- **Continuum toy model** (Levin 2006; Levin 2007)
  - Continuum of Alfvén oscillations
  - QPOs at turning points and edges
- **Linear simulations** (Sotani et al 2008; Colaiuda et al 2009)
  - Confirmation of Levin's model
  - overtone QPOs -> frequencies at integer multiples of fundamental frequency (agreement with observed QPOs)
- **Non-linear simulations** (anelastic approximation) (Cerdá-Durán et al 2009)

Our Alfvén QPO model

- Self-consistent equilibrium models (Bocquet et al 1995)
- Magstar (LORENE library) www.lorene.obspm.fr
- Non-rotating 1.4 $M_\odot$ NS + polytropic EOS
- Shear waves neglected + boundary condition for crust

Two complementary approaches:

1. Semi-analytical approach (short-wavelength approximation)

2. Non-linear MHD simulations

CoCoNuT code (Dimmelmeier, Font & Müller 2002, Cerdá-Durán et al 2008)

General Relativistic MHD code + dynamical spectime

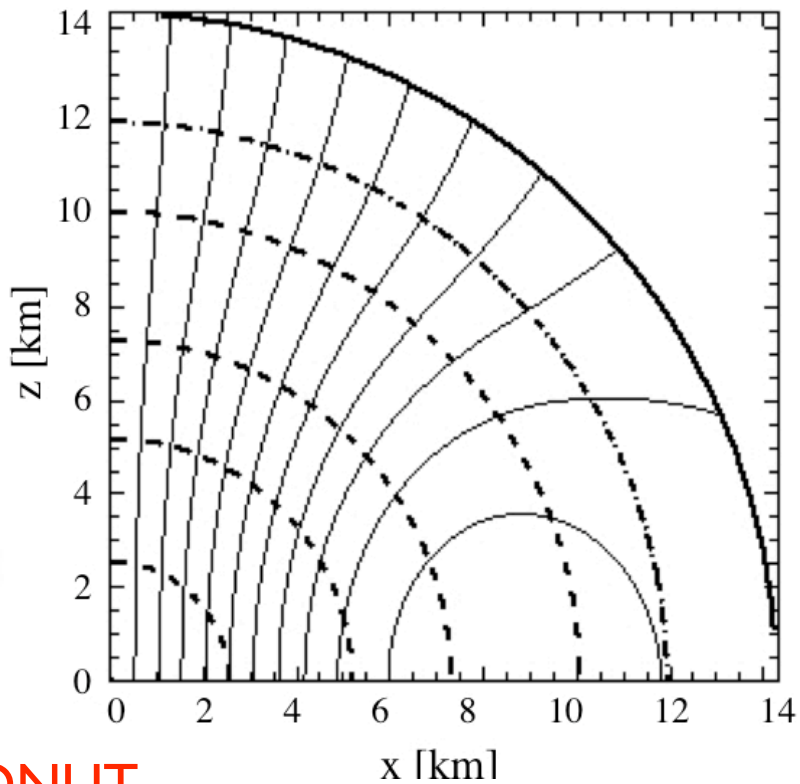

www.mpa-garching.mpg.de/Hydro/COCONUT

Semi-analytical approach

Idea: to compute Alfvén wave travel times along individual magnetic field lines (assuming a short-wavelength approximation).

Perturbations:

- propagate along magnetic field lines
- local Alfvén speed

Path of an Alfvén wave:

$$\frac{d\mathbf{x}}{dt} = \mathbf{v}_A(\mathbf{x}) \;\rightarrow\; \mathbf{x}(t_a, \mathbf{x}_0)$$

$\mathbf{x}_0$: starting point
t_a: arrival time

Open and closed magnetic field lines

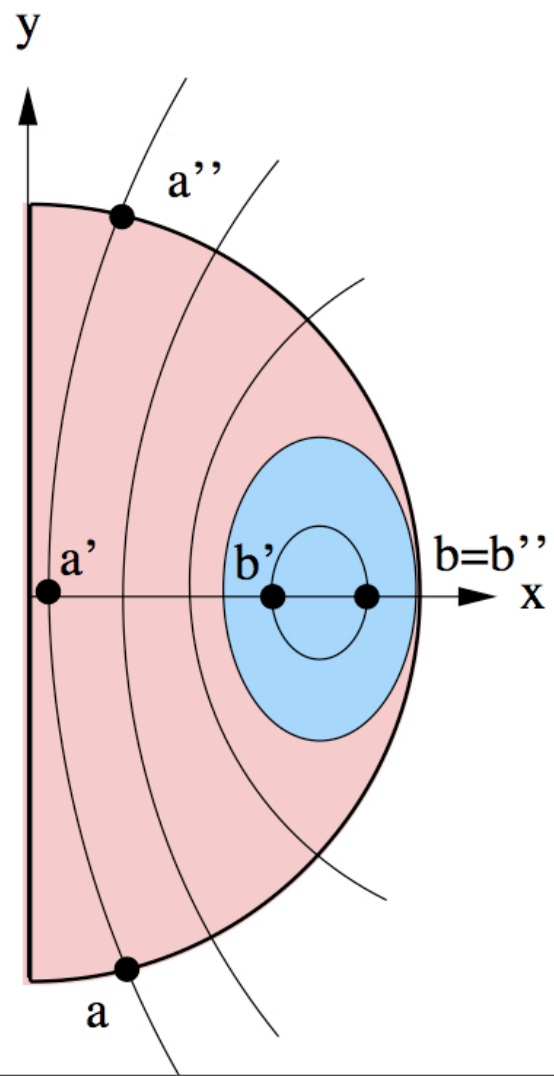

Semi-analytical approach

Coordinates adapted to the magnetic field lines

$$\mathbf{x}_0 \quad \rightarrow \quad \chi = \frac{r}{r_{\max}}$$ Position of the magnetic field line

$$t_{\mathrm{a}} \quad \rightarrow \quad \xi = \frac{t_{\mathrm{a}}}{t_{\mathrm{tot}}} - \frac{1}{2}$$ Location of points along an individual line

$$(r, \theta) \quad \rightarrow \quad (\chi, \xi)$$

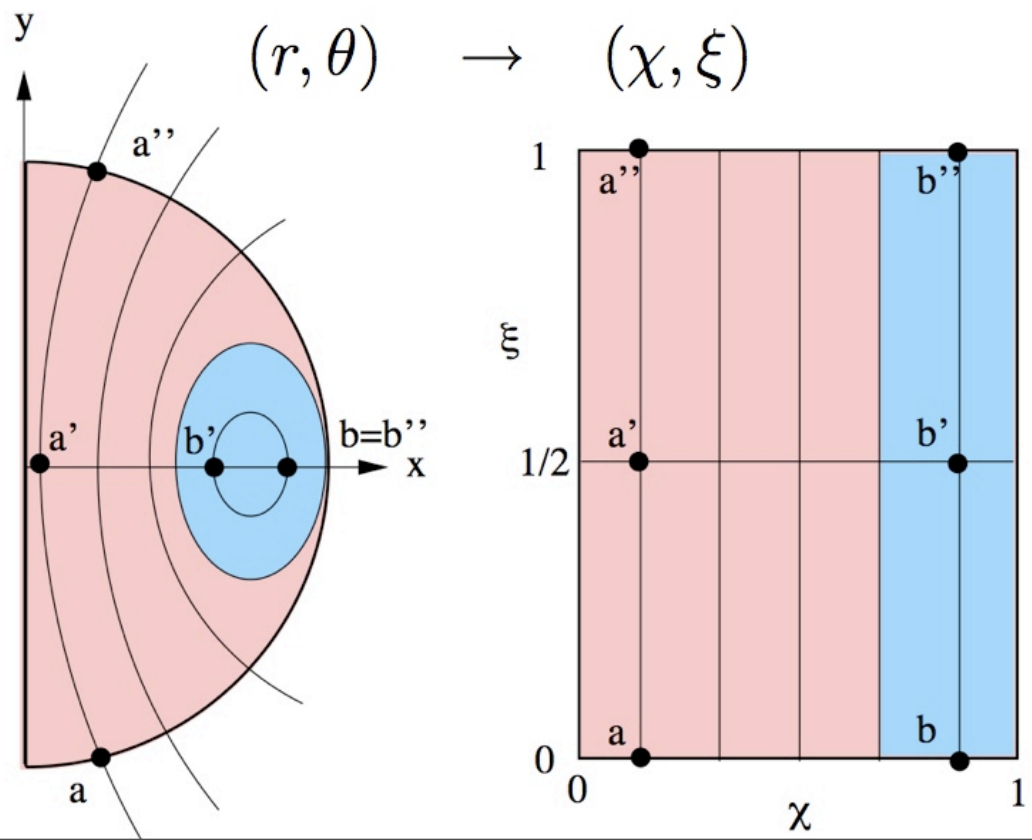

Displacement describing travelling waves along a specific line: $Y(\xi, \chi; t)$

$$\boxed{\frac{\partial^2 Y(\xi, t)}{\partial t^2} = \sigma^2 \frac{\partial^2 Y(\xi, t)}{\partial \xi^2}}$$

$$\sigma(\chi) = \frac{1}{t_{\mathrm{tot}}}$$ (wave speed)

Semi-analytical approach

$$\frac{\partial^2 Y(\xi,t)}{\partial t^2} = \sigma^2 \frac{\partial^2 Y(\xi,t)}{\partial \xi^2}$$

To find a correspondence with QPOs we are interested in solutions in the form of standing waves:

$$Y(\xi,t) = a\cos(k\xi+\phi)\sin(2\pi f t+\varphi)$$

initial conditions: amplitude, spatial phase, phase

boundary conditions: wave number, frequency

Semi-analytical approach

BC should ensure the continuity of traction at the surface. Since no magnetosphere dynamics included, traction must vanish at the surface.

Zero-traction boundary condition at the surface (open field lines)

$$\frac{\partial Y}{\partial r} = 0 \qquad \frac{\partial Y}{\partial \xi}\frac{\partial \xi}{\partial r} + \frac{\partial Y}{\partial \chi}\frac{\partial \chi}{\partial r} = 0$$

Applied to a standing-wave:

$$\left(2\pi t\frac{\partial f}{\partial \chi} + \frac{\partial \varphi}{\partial \chi}\right)\frac{\partial \chi}{\partial r} = 0 \qquad \frac{\partial a}{\partial \chi}\frac{\partial \chi}{\partial r} = 0$$

Two cases possible:

$$\frac{\partial f}{\partial \chi} = 0, \quad \frac{\partial \varphi}{\partial \chi} = 0, \quad \frac{\partial a}{\partial \chi} = 0$$

Turning-point (or constant) (Levin 2007)

$$\frac{\partial \chi}{\partial r} = 0$$

Magnetic field line perpendicular to NS surface (pole)

Semi-analytical approach

The time evolution of an initial perturbation will remain close to a standing wave solution as long as:

$$2\pi t \frac{\partial f}{\partial \chi} \ll 1, \quad \frac{\partial \varphi}{\partial \chi} \sim 0, \quad \frac{\partial a}{\partial \chi} \sim 0$$

Standing wave damping timescale (through phase mixing)

$$\boxed{\tau_{\mathrm{D}} = \frac{1}{2\pi}\left(\frac{\partial f}{\partial \chi}\right)^{-1}}$$

For timescales much smaller than the damping timescale one can define a *standing wave continuum of magnetic field lines* throughout the star, for each overtone:

Frequencies:

$$f(\chi) = \frac{n}{2t_{\mathrm{tot}}(\chi)}, \quad n = 1, 2, 3, 4, \cdots$$

QPO overtones appear at exact integer multiples of the corresponding fundamental frequency.

Semi-analytical approach

Standing-wave continuum & QPOs ($M=1.4M_{sun}$, $R=14.2$km, $B_{av}=4\times10^{15}$ G)

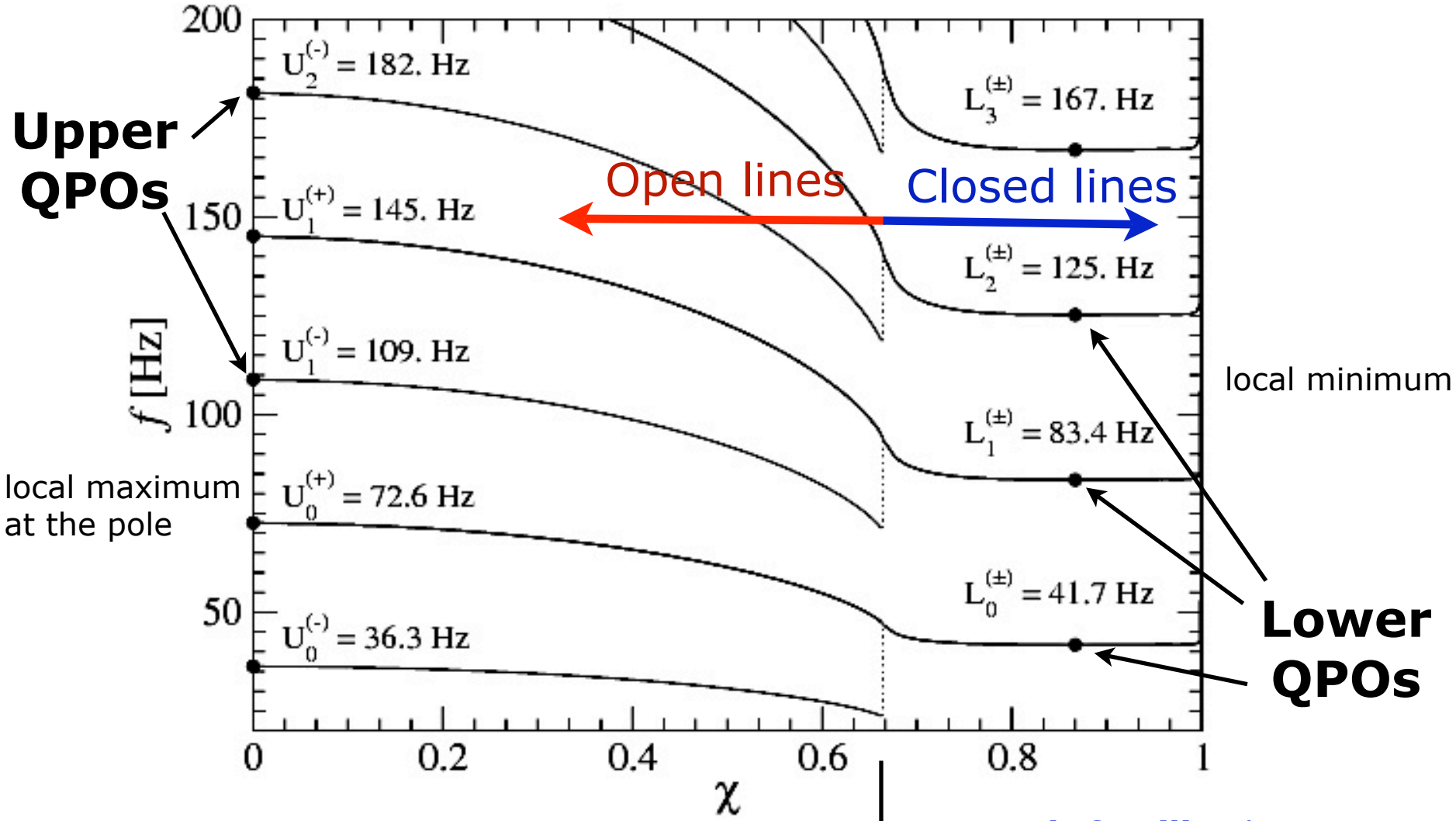

2 sub-families distinct freq.:
+ (-) symm. (antisymm.) across eq.

2 sub-families have identical frequencies

Numerical code: CoCoA/CoCoNuT

www.mpa-garching.mpg.de/Hydro/COCONUT

Developed for neutron star and gravitational core collapse studies

Spherical polar coordinates (2D, axisymmetry) + Ideal GRMHD

Godunov-type schemes for the GRMHD solver

- Approximate Riemann solvers
  - Complete: Marquina (only in hydro)
  - Incomplete: HLLE, Kurganov-Tadmor
- 2nd order cell reconstruction: MC, PHM
- Method of lines + 2nd order Runge-Kutta

CT scheme for the magnetic field

Spectral methods for the metric solver (elliptic part)

LORENE library

Brief history:

Dimmelmeier et al 2001, 2002ab (GRHD, 2D axisymmetric code)
Dimmelmeier et al 2005 (GRHD, 3D, spectral metric solver;MdM)
Cerdá-Durán et al 2005 (GRHD, 2D, CFC+)
Ott et al 2007a,b; Dimmelmeier et al 2007 (GRHD, 3D, microphysical EOS + deleptonization)
Cerdá-Durán et al 2007a,b (GRMHD, 2D, passive magnetic field)
Cerdá-Durán et al 2008 (GRMHD, 2D, active magnetic field)

General Relativistic Magneto-Hydrodynamics

Conservation of mass: $\nabla_\mu(\rho u^\mu) = 0$

Conservation of energy and momentum: $\nabla_\mu T^{\mu\nu} = 0$

Maxwell's equations: $\nabla_\mu {}^*F^{\mu\nu} = 0$ $\quad {}^*F^{\mu\nu} = \frac{1}{W}(u^\mu B^\nu - u^\nu B^\mu)$

- Divergence-free constraint: $\vec{\nabla} \cdot \vec{B} = 0$
- Induction equation: $\frac{1}{\sqrt{\gamma}}\frac{\partial}{\partial t}\left(\sqrt{\gamma}\vec{B}\right) = \vec{\nabla} \times \left[\left(\alpha\vec{v} - \vec{\beta}\right) \times \vec{B}\right]$

Adding all up: first-order, flux-conservative, hyperbolic system + constraint

$$\frac{1}{\sqrt{-g}}\left(\frac{\partial\sqrt{\gamma}\mathbf{U}}{\partial t} + \frac{\partial\sqrt{-g}\mathbf{F}^i}{\partial x^i}\right) = \mathbf{S} \qquad \frac{\partial(\sqrt{\gamma}B^i)}{\partial x^i} = 0$$

Antón et al. (2006)

$$D = \rho W \qquad S_j = \rho h^* W^2 v_j - \alpha b_j b^0 \qquad \tau = \rho h^* W^2 - p^* - \alpha^2 (b^0)^2 - D$$

$$\mathbf{U} = \begin{bmatrix} D \\ S_j \\ \tau \\ B^k \end{bmatrix} \quad \mathbf{F}^i = \begin{bmatrix} D\tilde{v}^i \\ S_j\tilde{v}^i + p^*\delta^i_j - b_j B^i/W \\ \tau\tilde{v}^i + p^* v^i - \alpha b^0 B^i/W \\ \tilde{v}^i B^k - \tilde{v}^k B^i \end{bmatrix} \quad \mathbf{S} = \begin{bmatrix} 0 \\ T^{\mu\nu}\left(\frac{\partial g_{\nu j}}{\partial x^\mu} - \Gamma^\delta_{\nu\mu} g_{\delta j}\right) \\ \alpha\left(T^{\mu 0}\frac{\partial \ln\alpha}{\partial x^\mu} - T^{\mu\nu}\Gamma^0_{\nu\mu}\right) \\ 0^k \end{bmatrix}$$

Magnetar models and main simplifications

Model	R_e [km]	r_e [km]	$r_p/r_e - 1$	M [$M_\odot$]	$B_{\rm polar}$ [G]	ρ_c[g cm^{-3}]	j_0 [A m^{-2}]	current function
MNS1	14.155	11.998	8×10^{-6}	1.40	6.5×10^{14}	7.91×10^{14}	2×10^{13}	Bocquet et al. (1995)
MNS2	14.157	11.999	8×10^{-4}	1.40	6.5×10^{15}	7.91×10^{14}	2×10^{14}	Bocquet et al. (1995)
MNS3	14.168	12.006	5×10^{-3}	1.40	1.6×10^{16}	7.91×10^{14}	5×10^{14}	Bocquet et al. (1995)
LMNS2	15.153	13.322	10^{-3}	1.20	5.1×10^{15}	5.47×10^{14}	2×10^{14}	Bocquet et al. (1995)
HMNS2	12.444	9.941	4×10^{-4}	1.60	8.4×10^{15}	1.37×10^{15}	2×10^{14}	Bocquet et al. (1995)
S1	14.153	11.912	0	1.40	4.0×10^{15}	7.91×10^{14}	N/A	Sotani et al. (2007a)

- Cowling approximation (fixed spacetime metric)
- Small-amplitude torsional perturbations
- Relativistic anelastic approximation (Bonazzola et al 2007)

➡ sound waves neglected (long-term evolutions)

$$Y(t=0) = 0 \quad \dot{Y}(t=0) = \alpha v^\varphi = f(r)\, b(\theta)$$

$$f(r) = \sin\left(\frac{3\pi}{2}\frac{r}{R}\right)$$

$$b(\theta) = b_2 \frac{1}{3}\partial_\theta P_2(\cos\theta) + b_3 \frac{1}{6}\partial_\theta P_3(\cos\theta)$$

Only left with evolution equations for S_φ and B^φ

$b_2=0$ ($b_3=0$) symm. (antisymm.) perturbation across equator

Anelastic approximation

Main idea (Bonazzola et al 2007): eliminate sound waves to reduce the time-step restrictions of numerical codes based on time-explicit schemes. Restrictions imposed by the dependence of the eigenvalues of the hyperbolic system on the speed of sound (see Antón et al 2006).

Modified equations: pressure terms in fluxes moved to sources. Leads to no sound speed dependence in eigenvalues.

$$\tilde{\boldsymbol{F}}^i = \left[D\hat{v}^i, S_j\hat{v}^i + \delta^i_j \frac{b^2}{2} - \frac{b_j B^i}{W}, \hat{v}^i B^k - \hat{v}^k B^i \right],$$

$$\tilde{\boldsymbol{S}} = \left[0, \frac{1}{2} T^{\mu\nu} \frac{\partial g_{\mu\nu}}{\partial x^j} - \frac{1}{\sqrt{-g}} \frac{\partial \sqrt{-g} P}{\partial x^i}, 0, 0, 0 \right].$$

New eigenvalues: $\tilde{\lambda}^i(\gamma_{ij}, \boldsymbol{U}) = \lambda^i(\gamma_{ij}, \boldsymbol{U}, c_s \to 0)$

Courant condition much less restrictive (not affected by sound waves)

Caution: we can use the anelastic approximation since we deal with low-amplitude torsional oscillations of an equilibrium star. They have axial parity and couple weakly to density perturbations (density and pressure can be considered constant).

Simulations: spatial pattern of effective amplitude

$$\mathcal{A}(r,\theta;f) = \mathrm{FT}\left[\dot{Y}(r,\theta;t)\right]$$

Amplitude only appreciable along magnetic axis

Non-zero (maximum) amplitude at the surface

Upper QPOs

Number of nodes along magnetic axis and location agrees with nodes computed with semi-analytic model

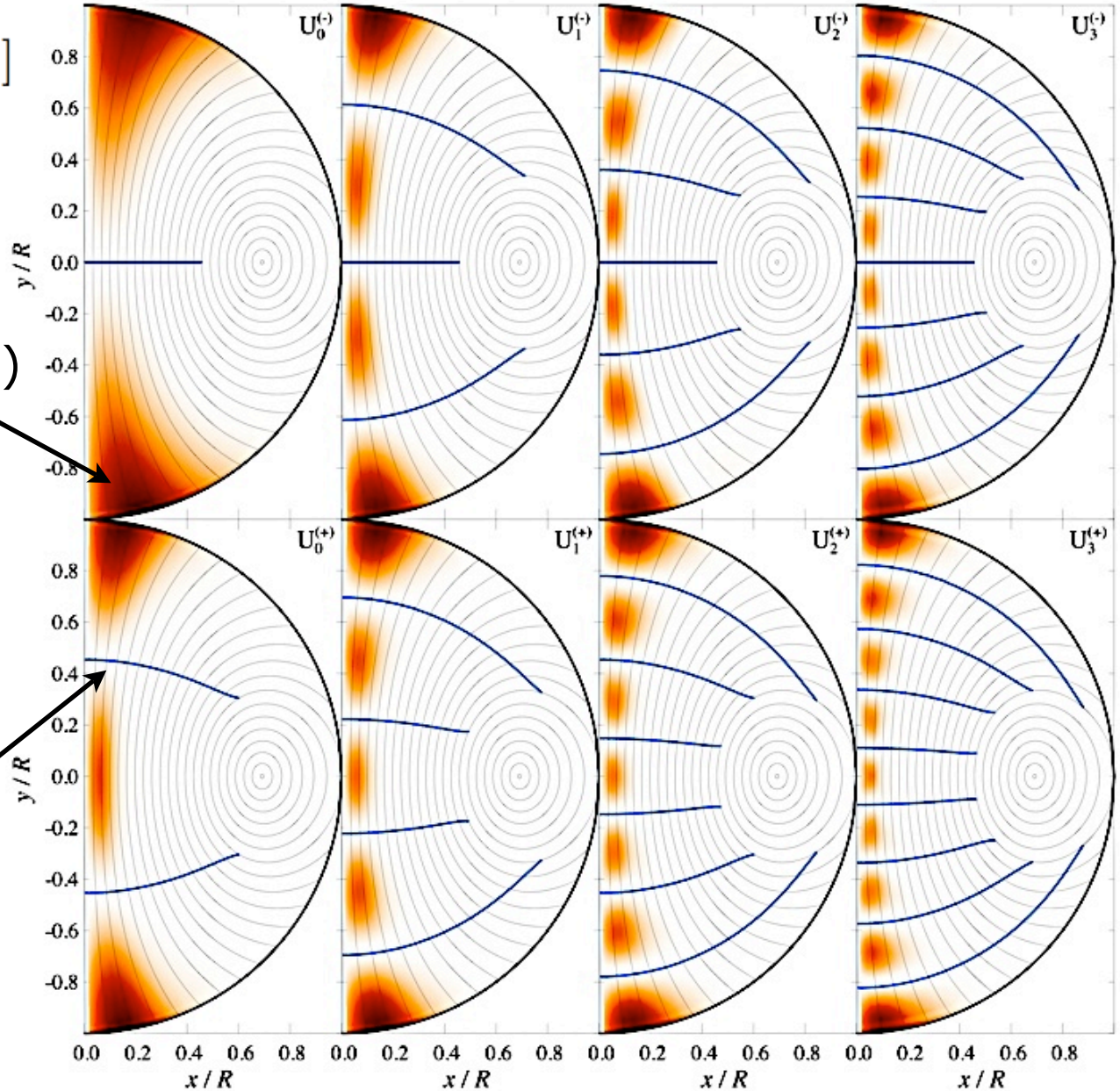

Simulations: spatial pattern of effective amplitude

Lower QPOs

Amplitude only appreciable within the region of closed field lines

QPO at the turning point

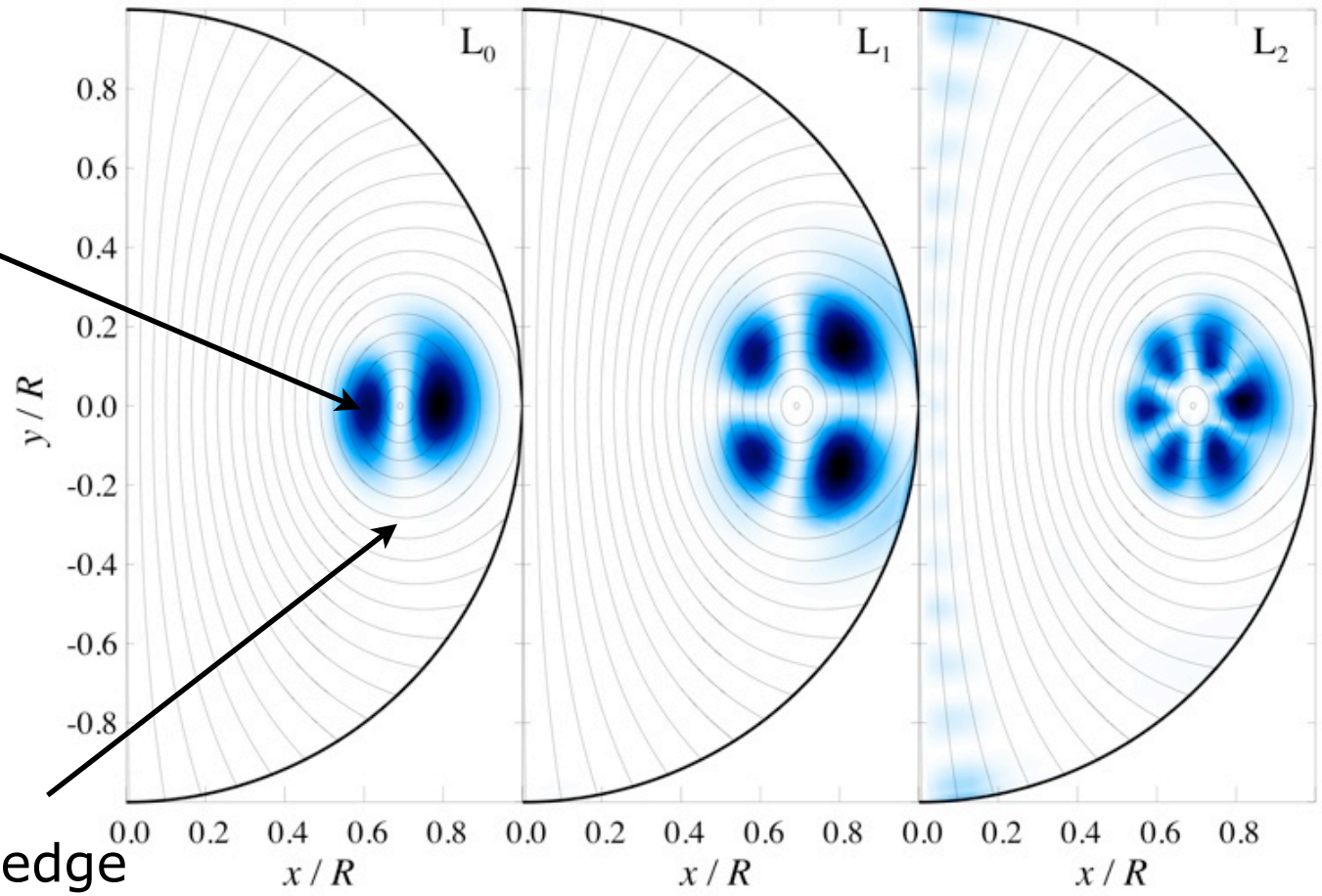

No QPO at the edge

(but Colaiuda et al 2009 find QPOs at the edge)

Numerical simulations

Time evolution maximum amplitude

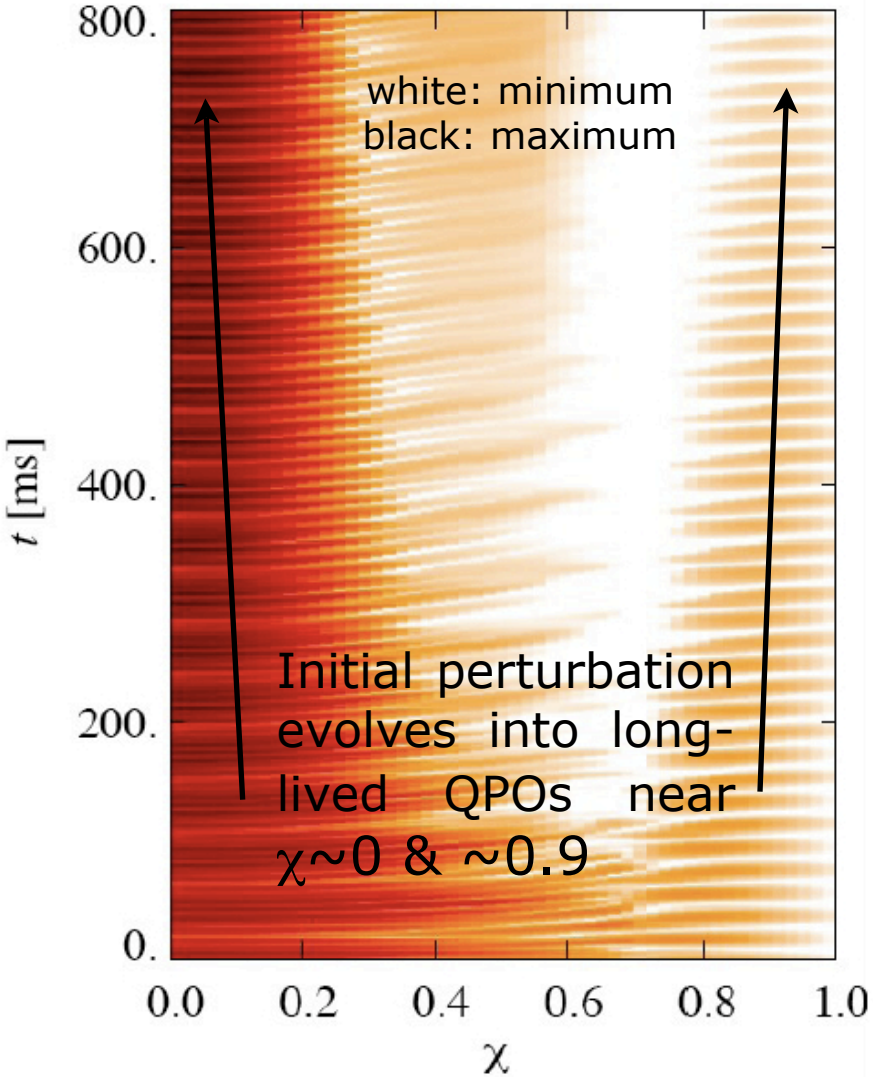

Spectrum average amplitude

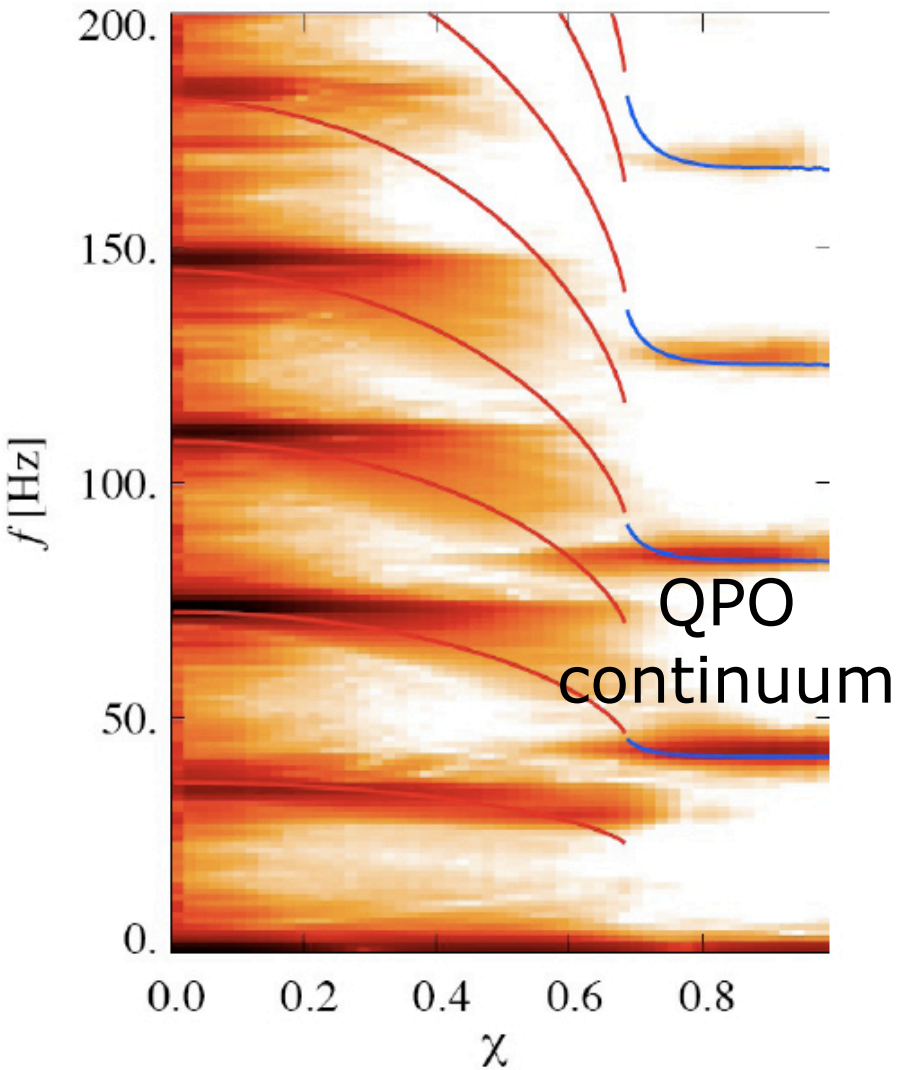

Numerical vs semi-analytical approach

QPO frequencies for reference model MNS2

"upper" QPOs	f (Hz)	"lower QPOs"	f (Hz)
$U_0^{(-)}$	35.1 (4.%) (*)	$L_0^{\pm}$	41.30 (1.0%)
$U_0^{(+)}$	72.6 (0.05%)	$L_1^{\pm}$	83.85 (0.6%)
$U_1^{(-)}$	110.2(1.1%)	$L_2^{\pm}$	126.4 (1.0%)
$U_1^{(+)}$	147.8(1.8%)	$L_3^{\pm}$	170.2 (2.0%)
$U_2^{(-)}$	182.8(0.7%)	$L_4^{\pm}$	210.3 (0.9%)
$U_2^{(+)}$	220.4(1.2%)	$L_5^{\pm}$	251.6 (0.6%)
$U_3^{(-)}$	256.7(1.0%)	$L_6^{\pm}$	295.4 (1.2%)
$U_3^{(+)}$	294.3(1.3%)	$L_7^{\pm}$	336.7 (0.9%)

Good agreement in both number and location of nodes, and frequencies (<2%)

relative difference w.r.t. semi-analytic approach

[(*) wavelength of standing-wave twice the size of the star (short-wavelength approx. innacurate)]

Empirical relations: magnetar asteroseismology

Our sample include models with either different central current density (MNS1 and MNS3) or central density (HMNS2 and LMNS2), wrt reference model MNS2.

Model	R_e [km]	r_e [km]	$r_p/r_e - 1$	M [$M_\odot$]	$B_{\rm polar}$ [G]	ρ_c[g cm^{-3}]	j_0 [A m^{-2}]	current function
MNS1	14.155	11.998	8×10^{-6}	1.40	6.5×10^{14}	7.91×10^{14}	2×10^{13}	Bocquet et al. (1995)
MNS2	14.157	11.999	8×10^{-4}	1.40	6.5×10^{15}	7.91×10^{14}	2×10^{14}	Bocquet et al. (1995)
MNS3	14.168	12.006	5×10^{-3}	1.40	1.6×10^{16}	7.91×10^{14}	5×10^{14}	Bocquet et al. (1995)
LMNS2	15.153	13.322	10^{-3}	1.20	5.1×10^{15}	5.47×10^{14}	2×10^{14}	Bocquet et al. (1995)
HMNS2	12.444	9.941	4×10^{-4}	1.60	8.4×10^{15}	1.37×10^{15}	2×10^{14}	Bocquet et al. (1995)
S1	14.153	11.912	0	1.40	4.0×10^{15}	7.91×10^{14}	N/A	Sotani et al. (2007a)

Agreement with Sotani et al (2008): our QPO frequencies change linearly with B and are consistent with their expansion in terms of the compactness (M/R). Allows to construct empirical relations for all QPO frequencies using those of Sotani et al (2008) constructed for a large set of tabulated EOS.

$$f_L = 56.8(n+1)\left[1 - 4.55\left(\frac{M}{R}\right) + 6.12\left(\frac{M}{R}\right)^2\right] \times \left(\frac{B}{4 \times 10^{15}\mathrm{G}}\right) \quad \text{(Hz)}$$

$$f_U = 48.9(n+1)\left[1 - 4.55\left(\frac{M}{R}\right) + 6.12\left(\frac{M}{R}\right)^2\right] \times \left(\frac{B}{4 \times 10^{15}\mathrm{G}}\right) \quad \text{(Hz)}$$

We use the set of models of Sotani et al (2008) for which the compactness ratio M/R ranges from 0.14 to 0.28.

SGR 1806-20: assuming that the observed frequencies of 30, 92 and 150Hz are produced as QPOs near the magnetic poles (upper QPOs) and are odd-integer multiples of the fundamental frequency of 30Hz, then the empirical relation restricts the dipolar component of the magnetic field to be in the range of 5×10^{15} G to 1.2×10^{16} G.

SGR 1900+14: if the observed frequencies of 28, 53, 84 and 155Hz are upper QPOs and near-integer multiples of the fundamental frequency of 28Hz, then the dipolar component of the magnetic field is in the range of 4.7×10^{15}G to 1.12×10^{16}G.

Mean surface magnetic field strength 3-8x10^{15}G (mean value at the surface is ~2/3 value at the pole)

Upper limit of the possible strength of the magnetic field, since the fundamental QPO frequencies could be any integer fraction of 30Hz in SGR 1806-20 or of 28Hz in SGR 1900+14.

Future extensions: crust inclusion

Work performed by M. Gabler (MPA; PhD advisor E. Müller)

Status:

- Linearized equation for the evolution of the perturbation in terms of traction and displacement derived.
- Tabulated EOS of Douchin and Haensel (2001) for the crust and density-dependent shear modulus computed following Piro (2005) and Sotani et al (2007). Pure crustal frequencies for linearized eq. computed. Broad agreement with Samuelsson and Andersson 2007.
- Boundary conditions derived: continuous traction condition at both sides of the crust (surface and crust-core interface).
- Currently comparing evolution of linearized equation with full nonlinear code for a vanishing shear modulus. Work in progress.

Summary

- Study of Alfvén oscillations in magnetars using semi-analytic approach and nonlinear MHD simulations (anelastic approximation).
- Alfvén oscillations form a continuum in the core of magnetars. QPOs correspond to turning points of the continuum.
- Two families of QPOs with harmonics at integer multiples of the fundamental frequency.
- Crust-core coupling induces strong damping.
- Short-wavelength approximation can be used to compute QPO frequencies without numerical simulations to high accuracy.
- Empirical relations applied to SGR 1806-20 and SGR 1900+14 yield upper limits to mean surface (dipolar) magnetic field strength $3\text{-}8\times10^{15}$G.

- Inclusion of crust performed, code validation in progress.
- Magnetosphere will be incorporated next (mid-term project).